ChemComm

COMMUNICATION

View Article Online
View Journal | View Issue

Cite this: *Chem. Commun.*, 2015, 51, 8640

Received 8th March 2015,
Accepted 14th April 2015

DOI: 10.1039/c5cc01966d

www.rsc.org/chemcomm

Efficient room temperature aqueous Sb_2S_3 synthesis for inorganic–organic sensitized solar cells with 5.1% efficiencies†

Karl C. Gödel,[a] Yong Chan Choi,[b] Bart Roose,[ac] Aditya Sadhanala,[a] Henry J. Snaith,[d] Sang Il Seok,[be] Ullrich Steiner*[c] and Sandeep K. Pathak[ad]

Sb_2S_3 sensitized solar cells are a promising alternative to devices employing organic dyes. The manufacture of Sb_2S_3 absorber layers is however slow and cumbersome. Here, we report the modified aqueous chemical bath synthesis of Sb_2S_3 absorber layers for sensitized solar cells. Our method is based on the hydrolysis of $SbCl_3$ to complex antimony ions decelerating the reaction at ambient conditions, in contrast to the usual low temperature deposition protocol. This simplified deposition route allows the manufacture of sensitized mesoporous-TiO_2 solar cells with power conversion efficiencies up to η = 5.1%. Photothermal deflection spectroscopy shows that the sub-bandgap trap-state density is lower in Sb_2S_3 films deposited with this method, compared to standard deposition protocols.

Antimony sulfide (Sb_2S_3) is a promising material for several optoelectronic applications. Due to its high absorption coefficient ($\alpha \approx 1.8 \times 10^5$ cm^{-1} at λ = 450 nm) and a suitable direct band-gap of $E_g \approx 1.7$ eV, crystalline Sb_2S_3 (stibnite) is interesting as light absorber for solid-state sensitized solar cells (Fig. 1).[1,2] In particular, Sb_2S_3-based solar cells excel in their stability of operation when compared to other organic–inorganic hybrid devices. Recently, power-conversion efficiencies of η = 6.2% (ref. 3) and η = 7.5% (ref. 4) were achieved using Sb_2S_3 as the absorber material obtained from chemical bath deposition. Further, the material has been used to improve the stability of methyl-ammonium lead iodide perovskite solar cells.[5]

Antimony sulfide synthesis typically involves deposition in aqueous and non-aqueous chemical baths at low temperatures (low-T deposition).[6–9] The standard method is the aqueous chemical bath deposition (CBD) using antimony chloride and sodium thiosulfate. This technique is however problematic since it requires a precise temperature control of the solution when cooling below 10 °C and maintaining the sample at low temperatures. For large-scale applications such a cooling protocol is cumbersome, costly and energy-intensive.

Here, we present an aqueous room temperature (RT) deposition route of Sb_2S_3 using the same precursor materials as the standard CBD method. We have fabricated Sb_2S_3-sensitized

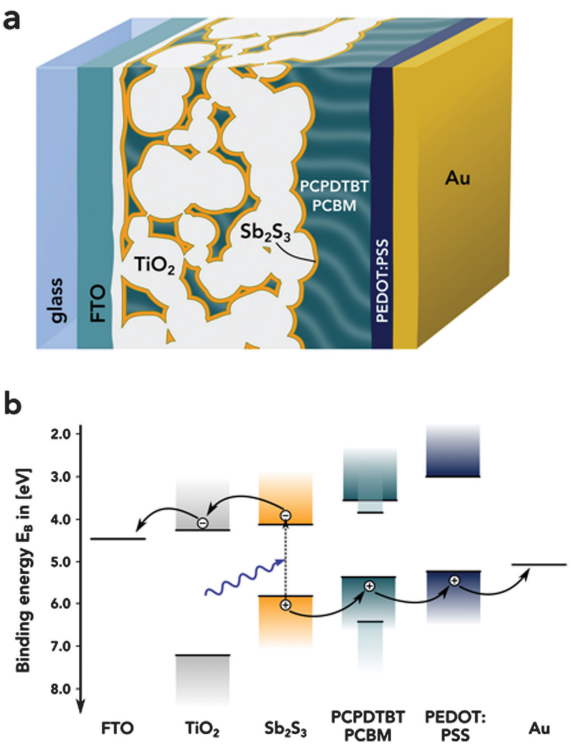

Fig. 1 (a) Schematic of the solar cell cross section. (b) Simplified band-diagram of the Sb_2S_3 sensitised photovoltaic cells. The band edge values were taken from ref. 10.

[a] *Cavendish Laboratory, Department of Physics, University of Cambridge, J J Thomson Avenue, Cambridge CB3 0HE, UK*
[b] *Division of Advanced Materials, Korea Research Institute of Chemical Technology, 141 Gajeong-Ro, Yuseong-Gu, Daejeon 305-600, Republic of Korea*
[c] *Adolphe Merkle Institute, Rue des Verdiers 4, CH-1700 Fribourg, Switzerland. E-mail: ullrich.steiner@unifr.ch*
[d] *Clarendon Laboratory, Department of Physics, University of Oxford, Parks Road, Oxford, OX1 3PU, UK*
[e] *Department of Energy Science, Sungkyunkwan University, 2066 Seoburo, Jangsan-gu, Suwon 440-746, Republic of Korea*

† Electronic supplementary information (ESI) available. See DOI: 10.1039/c5cc01966d

solar cells using this RT deposition method and demonstrate excellent device performance with efficiencies of up to $\eta = 5.1\%$.

The low-temperature synthesis of Sb_2S_3 for photovoltaic applications involves the chemical reaction equations[7]

$$2SbCl_3 + 3Na_2S_2O_3 \rightarrow Sb_2(S_2O_3)_3 + 6NaCl$$

$$Sb_2(S_2O_3)_3 + 6H_2O \rightarrow Sb_2S_3 + 3HSO_4^- + 3H_3O^+.$$

These reactions have to be slowed down by cooling below 10 °C to avoid immediate precipitation[7] and to enable strong adhesion of Sb_2S_3 to the substrate. Thus, the standard CBD method, termed low-T deposition, requires cooling of the reaction solution, whereas our modified method, RT deposition, can be performed at room temperature. By changing the order of reactant addition at RT, Sb_2S_3 formation is slowed down and well-adhering films are obtained.

For the RT deposition, a 1.4 M $SbCl_3$ solution in acetone was prepared. Note that the optimal concentration of $SbCl_3$ for the RT method is slightly higher compared to low-T deposition (Fig. S7, ESI†). $SbCl_3$ can be used without dissolution in acetone, changing the reaction behaviour very little (Fig. S8, ESI†). The addition of acetone facilitates however the handling of the highly hygroscopic $SbCl_3$. Deionised water is added under vigorous stirring to reduce the total concentration of $SbCl_3$ to 46 mM. The addition of water hydrolyses $SbCl_3$, which leads to a solid white precipitate. The product of the hydrolysis reaction of $SbCl_3$ is not very well defined. It depends on many parameters such as the dilution of the reaction medium, the pH value of the solution and solvent composition.[11,12] The aqueous solution containing the hydrolysed $SbCl_3$ has a pH of 1.4.

The precipitate was filtered and dried and X-ray diffraction (XRD), Fourier transform infrared spectroscopy (FTIR) and energy-dispersive X-ray (EDX) spectroscopy were performed on the white powder (Fig. S10–S12, ESI†). The XRD pattern shows crystalline phases of $Sb_4O_5Cl_2$, $Sb_8(OH)_6O_8Cl_2(H_2O)$, $Sb_8O_{11}Cl_2(H_2O)_6$ and $Sb_3O_6(OH)$. This is in contrast to the reports by Li *et al.* and Yu *et al.* describing similar reactions.[13,14] They also reporting the formation of a white precipitate, which they identify as antimony oxychloride SbOCl. The XRD pattern of Fig. S10 (ESI†) however shows no evidence of crystalline SbOCl formation. According to Chen *et al.* hydrolysis at pH 1–2 leads to the formation of $Sb_4O_5Cl_2$ for mixed solvents such as water and ethanol or water and ethylene glycol.[12] We also do not observe an immediate colour change of the precipitate to orange upon the addition of the sulphur source, as reported by Li *et al.*[13] and Yu *et al.*[14]

Subsequently, a 1 M aqueous $Na_2S_2O_3$ solution was added at a final concentration of 0.25 M in the chemical bath. This causes the solution to turn clear as most of the precipitate dissolves, suggesting the formation of a water-soluble complex. After 5–10 min at 20 °C, the solution starts to turn orange, indicating the formation of amorphous Sb_2S_3. This is accompanied by a pH change of the solution from pH = 3.3 upon sodium thiosulfate (pH = 7.3) addition to pH = 4.3 when antimony sulfide deposition is complete after two hours.

Fig. S2 (ESI†) shows the UV-vis spectra of RT-deposited Sb_2S_3 films on mesoporous-TiO_2, annealed at 300 °C for 5 min.

The annealed antimony sulfide was characterised by powder X-ray diffraction (XRD). Fig. 3a compares the XRD pattern of the low-T and RT deposition methods. Both pattern are very similar and match the stibnite reference pattern.[15] Sb_2S_3 films deposited by the RT method onto mesoporous TiO_2 substrates also show the characteristic XRD peaks of crystalline Sb_2S_3 (Fig. S3, ESI†). A Rietveld analysis of the two patterns using the powder diffraction software ReX[16] yields an average Sb_2S_3 crystallite size of 40 nm and 35 nm for RT and low-T deposition, respectively. The structure of the solar cell studied in this work and a schematic band diagram are shown in Fig. 1.

Fig. 2 shows (a) the current–voltage-characteristic and (b) the external quantum efficiency EQE of the best performing solar cell employing RT deposited Sb_2S_3. Its photovoltaic parameters are summarised in Fig. 2. The shunt and series resistances were obtained by a least square fit of the diode function. The RT method enables the fabrication of solar cells with high reproducibility. The deviations from batch to batch and from device to device were small (Fig. S13, ESI†). The hole transport layer consists of a PCPDTBT–PCBM blend. Charge carriers which are generated by photon absorption in the hole transport

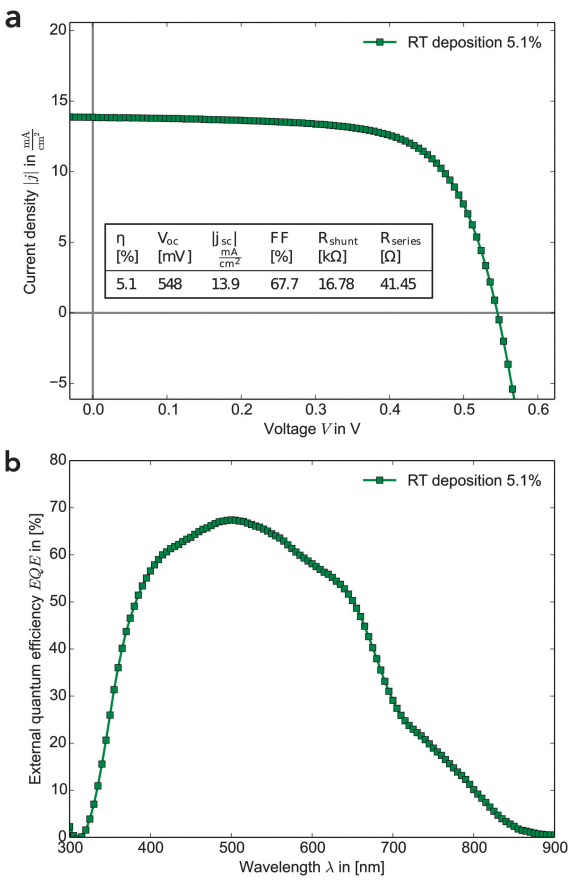

Fig. 2 (a) Current–voltage curve of the best performing solar cell device employing Sb_2S_3 synthesised using the RT method. The inset table shows the photovoltaic parameters of the device. (b) External quantum efficiency of the device.

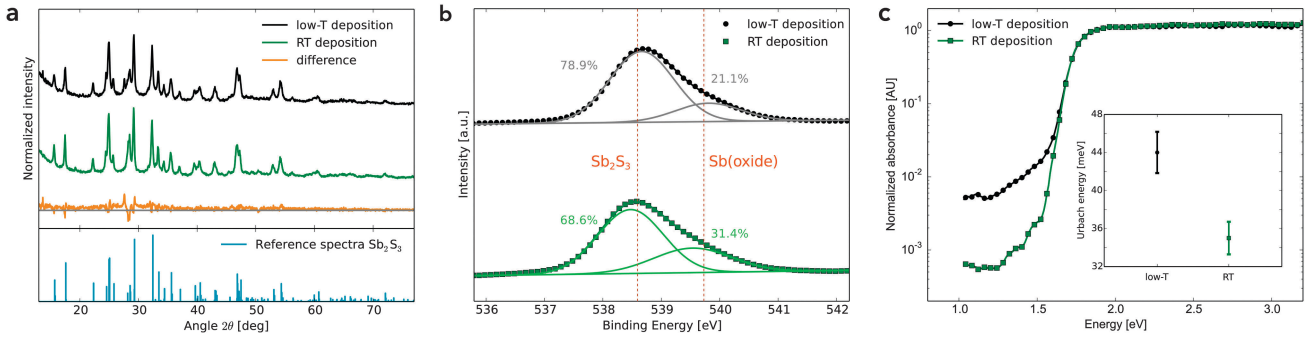

Fig. 3 (a) XRD pattern of crystalline Sb_2S_3, synthesised *via* the low temperature deposition method (upper trace) and the RT technique (center trace). The lower trace shows the difference of the two patterns. The stibnite reference pattern was taken from ref. 15. (b) XPS $Sb3d_{3/2}$ peak of films from both deposition methods. The solid lines show a least squares fit of a superposition of two Gaussian curves. (c) PDS measurements showing the sub band-gap energy levels for both deposition methods. The inset shows the corresponding Urbach energies.

layer can also be harvested due to the formation of PCBM electron conducting channels. The PCBM–PCPDTBT blend thus contributes to the current and causes the near-infrared shoulder in the EQE spectrum.[17] Earlier cells using P3HT as hole conductor showed lower efficiencies compared to the PCPDTBT:PCBM blend. We therefore concentrated on the donor–acceptor PCPDTBT–PCBM blend. A comparison of a RT solar cell and a solar cell with the same device architecture using the low-temperature deposition method is shown in the ESI† (Fig. S4). The reference cells were prepared in the same laboratory using the identical procedures as the better performing earlier published devices.[4] The lower performance may reflect the variation in this system that possibly arises from minor variations in device fabrication. It is however important to point out that the reference devices and devices made with our new methodology were created in parallel and therefore are much less likely to be subject to this type of variation.

X-ray photoelectron spectroscopy (XPS) measurements were carried out on Sb_2S_3 films formed by both deposition techniques, shown in Fig. 3b.

To compare the oxide content of the samples, the antimony $Sb3d_{3/2}$ peak was examined, because the oxygen O1s peak directly overlaps with the antimony $Sb3d_{5/2}$ peak. The $Sb3d_{3/2}$ peak can be modelled using a superposition of two Gaussians, one at $\approx$538.5 eV representing Sb_2S_3 and one at $\approx$539.5 eV for SbO_x, most likely Sb_2O_3.[18] The RT sample has a marginally higher oxide content compared to the low-T material. This probably causes the lower conductivity seen in these films (Fig. S6, ESI†).

One of the biggest challenges of using antimony sulfide as absorber in sensitized solar cells is the high density of electronic traps in this material, *i.e.* the number of energy states which lie in the band-gap of Sb_2S_3.[4,19] These trap-states lead to a significant loss in potential and to charge carrier recombination in the solar cell. To explore this, we employed photo-thermal deflection spectroscopy (PDS) to determine the trap-state density and the energetic disorder of Sb_2S_3. PDS is a highly sensitive absorption measurement technique, which can detect absorbance values down to 10^{-5} AU. Thus, PDS is able to accurately measure weak absorption in the bandgap. Fig. 3c shows the PDS spectra of Sb_2S_3 samples on mesoporous TiO_2 for both deposition methods. The corresponding Urbach energies are given in the inset.

The absorption in the RT-deposited sample was significantly lower at energies below the band-gap of Sb_2S_3 compared to the low-T sample, by nearly one order of magnitude at energies below 1.5 eV. This indicates a clear reduction in the density of deep-trap states for the RT deposited Sb_2S_3. The difference in the open-circuit voltage for low-T and RT deposited Sb_2S_3 in optimized solar cells are however similar (Fig. S4, ESI†). As the band-gap of antimony oxide is higher than that of Sb_2S_3,[20] the PDS spectrum cannot show a potential increase of deep traps caused by the higher content of antimony oxide in the RT-deposited sample.

We have demonstrated an aqueous deposition technique of antimony sulfide for sensitized solar cells, which can be carried out at room temperature. The chemical bath deposition method is based on the same precursor materials but uses the hydrolysis of $SbCl_3$ to complex antimony ions. The resulting Sb_2S_3 films were investigated using UV-vis spectroscopy, XRD, PDS and XPS. PDS shows a reduction in sub-band gap trap states in RT-deposited Sb_2S_3. Manufactured devices achieved a maximum power conversion efficiency η = 5.1% for Sb_2S_3 sensitized solar cells using the RT deposition method. A more detailed optimization of the deposition step, interfacial surface treatments[21,22] or doping of the Sb_2S_3[23] could lead to a further improvement in solar cell performance. This work is therefore an important step in the development of low-cost, stable and highly efficient solar cells.

We acknowledge Adam Brown's help with the XPS measurements. K.C.G. would like to thank the Cambridge Trust, the Mott Fund for Physics of the Environment and Corpus Christi College Cambridge for funding. A.S. acknowledges funding from the Engineering and Physical Sciences Research Council (EPSRC).

References

1 M. Y. Versavel and J. A. Haber, *Thin Solid Films*, 2007, **515**, 7171–7176.
2 S.-J. Moon, Y. Itzhaik, J.-H. Yum, S. M. Zakeeruddin, G. Hodes and M. Grätzel, *J. Phys. Chem. Lett.*, 2010, **1**, 1524–1527.
3 S. H. Im, C.-S. Lim, J. A. Chang, Y. H. Lee, N. Maiti, H.-J. Kim, M. K. Nazeeruddin, M. Grätzel and S. I. Seok, *Nano Lett.*, 2011, **11**, 4789–4793.
4 Y. C. Choi, D. U. Lee, J. H. Noh, E. K. Kim and S. I. Seok, *Adv. Funct. Mater.*, 2014, **24**, 3587–3592.

5 S. Ito, S. Tanaka, K. Manabe and H. Nishino, *J. Phys. Chem. C*, 2014, **118**, 16995–17000.
6 I. Grozdanov, *Semicond. Sci. Technol.*, 1994, **9**, 1234.
7 M. T. S. Nair, Y. Pena, J. Campos, V. M. Garcia and P. K. Nair, *J. Electrochem. Soc.*, 1998, **145**, 2113–2120.
8 S. Messina, M. Nair and P. Nair, *Thin Solid Films*, 2007, **515**, 5777–5782.
9 N. Maiti, S. H. Im, C.-S. Lim and S. I. Seok, *Dalton Trans.*, 2012, **41**, 11569–11572.
10 J. A. Chang, J. H. Rhee, S. H. Im, Y. H. Lee, H.-j. Kim, S. I. Seok, M. K. Nazeeruddin and M. Gratzel, *Nano Lett.*, 2010, **10**, 2609–2612.
11 A. Koliadima, A. Henglein and E. Matijević, *Colloid Polym. Sci.*, 1997, **275**, 972–978.
12 X. Y. Chen, H. S. Huh and S. W. Lee, *J. Solid State Chem.*, 2008, **181**, 2127–2132.
13 C. Li, X. Yang, Y. Liu, Z. Zhao and Y. Qian, *J. Cryst. Growth*, 2003, **255**, 342–347.
14 Y. Yu, R. H. Wang, Q. Chen and L.-M. Peng, *J. Phys. Chem. B*, 2005, **109**, 23312–23315.
15 A. Kyono and M. Kimata, *Am. Mineral.*, 2004, **89**, 932–940.
16 M. Bortolotti, L. Lutterotti and I. Lonardelli, *J. Appl. Crystallogr.*, 2009, **42**, 538–539.
17 J. A. Chang, S. H. Im, Y. H. Lee, H.-J. Kim, C.-S. Lim, J. H. Heo and S. I. Seok, *Nano Lett.*, 2012, **12**, 1863–1867.
18 V. P. Zakaznova-Herzog, S. L. Harmer, H. W. Nesbitt, G. M. Bancroft, R. Flemming and A. R. Pratt, *Surf. Sci.*, 2006, **600**, 348–356.
19 A. Darga, D. Mencaraglia, C. Longeaud, T. J. Savenije, B. O'Regan, S. Bourdais, T. Muto, B. Delatouche and G. Dennler, *J. Phys. Chem. C*, 2013, **117**, 20525–20530.
20 Z. Deng, F. Tang, D. Chen, X. Meng, L. Cao and B. Zou, *J. Phys. Chem. B*, 2006, **110**, 18225–18230.
21 K. Tsujimoto, D.-C. Nguyen, S. Ito, H. Nishino, H. Matsuyoshi, A. Konno, G. R. A. Kumara and K. Tennakone, *J. Phys. Chem. C*, 2012, **116**, 13465–13471.
22 T. Fukumoto, T. Moehl, Y. Niwa, M. K. Nazeeruddin, M. Grätzel and L. Etgar, *Adv. Energy Mater.*, 2013, **3**, 29–33.
23 S. Ito, K. Tsujimoto, D.-C. Nguyen, K. Manabe and H. Nishino, *Int. J. Hydrogen Energy*, 2013, **38**, 16749–16754.